ISSN 0106 - 2646

NORDITA preprint

NORDITA - 94/76 N

THREE-BODY STRUCTURE OF ^{8}LI AND THE ^{7}LI(N,γ)^{8}LI REACTION

N.B. Shul'gina*, Nordita, Blegdamsvej 17, DK-2100 Copenhagen Ø, Denmark.

B.V. Danilin†, Chalmers Univ. of Technology, S-41296 Göteborg, Sweden and Nordita.

V.D. Efros‡, The Niels Bohr Institute and Nordita, Blegdamsvej 17, DK-2100 Copenhagen Ø, Denmark.

J. Bang, The Niels Bohr Institute, Blegdamsvej 17, DK-2100 Copenhagen Ø, Denmark.

J. Vaagen, Nordita, Blegdamsvej 17, DK-2100 Copenhagen Ø, Denmark and permanent address: SENTEF, Dept. of Physics, Univ. of Bergen, Norway.

M. Zhukov, Chalmers Univ. of Technology and Göteborg Univ., S-41296 Göteborg, Sweden.

*,†,‡Permanent address: The Kurchatov Institute, Kuchatov Sq.1, 123182, Moscow, Russia.

NORDITA · Nordisk Institut for Teoretisk Fysik

Blegdamsvej 17 DK-2100 København Ø Danmark

THREE-BODY STRUCTURE OF ^{8}Li AND THE ^{7}Li(n,γ)^{8}Li REACTION

Russian-Nordic-British Theory (RNBT) collaboration

N.B.Shul'gina*
NORDITA, Blegdamsvej 17, DK-2100 Copenhagen Ø, Denmark

B.V.Danilin†
Chalmers University of Technology, S-41296 Göteborg, Sweden and NORDITA

V.D.Efros‡
The Niels Bohr Institute and NORDITA, Blegdamsvej 17, DK-2100 Copenhagen Ø, Denmark

J.M.Bang
The Niels Bohr Institute, Blegdamsvej 17, DK-2100 Copenhagen Ø, Denmark

J.S.Vaagen§
NORDITA, DK-2100 Copenhagen Ø, Denmark

M.V.Zhukov
Chalmers University of Technology and Göteborg University, S-41296 Göteborg, Sweden

*Permanent address: The Kurchatov Institute, Kurchatov Sq.1, 123182, Moscow, Russia
†Permanent address: The Kurchatov Institute, Kurchatov Sq.1, 123182 Moscow, Russia
‡Permanent address: The Kurchatov Institute, Kurchatov Sq.1, 123182, Moscow, Russia
§Permanent address: SENTEF Department of Physics, University of Bergen, Norway

Abstract

A microscopic three-body cluster ^{4}He+t+n model is developed for ^{8}Li using the method of hyperspherical harmonics with cluster interactions fitted to experimental data. The model is used to calculate wave functions, spatial and matter densities of the ground state and the low lying excited state of ^{8}Li. The model reproduces experimentally known properties of ^{8}Li. Contrary to two-body models, our prediction for the radiative neutron capture on ^{7}Li at low energies supports a lower cross section value.

1 Introduction

The trigger reactions to nucleosynthesis proceed via light nuclei, which are known to have a cluster nature. Few-body models of light nuclei have been intensively developed in the last decade, as reviewed in [1]. Thorough investigations of A=6 nuclei and ^{11}Li in three-body models [2] have shown that essential characteristics are well accounted for. The three-particle structure and three-particle asymptotic behaviour is of particular importance for nuclear reactions at energies of astrophysical interest.

The nuclear structure of the A=8 nuclei ^{8}Li (and ^{8}B) can, as we will show below, also be considered in a three-body approach. It is a question of interest not only in nuclear physics but even more so in astrophysics and weak interaction physics. This paper investigates ^{8}Li, which will be considered as a three-particle (^{4}He + t + n) system. Here the Coulomb part is essentially simpler than for the isospin mirror nucleus ^{8}B. It is natural to expect that the structure of ^{8}B should have similarities with that of ^{8}Li. The rate of the ^{7}Be + p = ^{8}B +γ reaction, relevant for the Solar neutrino problem, could be strongly affected by specific three-particle features of ^{8}B (^{4}He + ^{3}He + p). The exact solution of this particular three-body problem implies the exact reproduction of two-particle (^{7}Be+p) asymptotic behaviour of the wave function as well as a solution of the difficult three-body Coulomb problem. We will return to this in a forthcoming publication.

The ^{8}Li structure is important not only as a doorway to understanding the ^{7}Be + p reaction mechanism: The radiative capture ^{7}Li+n =^{8}Li + γ is in fact the trigger reaction to the primordial nucleosynthesis of heavy elements in inhomogenous big-bang models [6] due to the chain: ^{7}Li(n,γ) ^{8}Li(^{4}He,n) ^{11}B(n,γ) ^{12}B(β)^{12}C with "leak" to the chain ^{8}Li(n,γ)^{9}Li(β^-,ν)^{9}Be(p,α)^{6}Li. The experimental status of the ^{7}Li+n=^{8}Li+γ reaction is regrettably not clear. The three experiments on the thermal radiative neutron capture [3, 4, 5] only agree with each other within a factor of two.

2 Theoretical background

Within the cluster representation of $A = 8$ nuclei (see Refs.[1], [2] for details), three-body bound state and continuum center-of - mass system wave functions (WFs) have the form

of products of intrinsic cluster WFs and functions of the relative motion coupled to total angular momentum J, M and isospin T, M_T,

$$\Phi_{JMTM_T} = \Phi_\alpha(\zeta_\alpha) \sum_{L,S} \Big[\Psi_L^S(\mathbf{x},\mathbf{y}) \cdot \Big[\Phi_t^{S_t T_t}(\zeta_t) \cdot \chi_n^{S_n T_n} \Big]_{ST} \Big]_{JM} \tag{1}$$

where $\Phi_\alpha(\zeta_\alpha)$ and $\Phi_t^{S_t T_t}(\zeta_t)$ are intrinsic WFs of ^{4}He and t respectively, $\chi_n^{S_n T_n}$ are the neutron spin-isospin functions, L and S are net orbital momentun and spin quantum numbers and the brackets [...] mean a vector coupling. Functions $\Psi_L^S(\mathbf{x},\mathbf{y})$ describe the three-cluster relative motion.

Translationally invariant normalized sets of Jacobi coordinates $\mathbf{x}$ and $\mathbf{y}$ are defined as follows

$$\mathbf{x}_3 = (A_{12})^{1/2}\mathbf{r}_{12} = (A_{12})^{1/2}(\mathbf{R}_2 - \mathbf{R}_1),$$
$$\mathbf{y}_3 = (A_{(12)3})^{1/2}\mathbf{r}_{(12)3} = (A_{(12)3})^{1/2}[-\mathbf{R}_3 + (A_1\mathbf{R}_1 + A_2\mathbf{R}_2)/(A_1 + A_2)], \tag{2}$$

Here $A_{12} = A_1A_2/(A_1 + A_2)$ is the reduced mass of the (12) subsystem in units of the nucleon mass m, $A_{(12)3} = (A_1 + A_2)A_3/(A_1 + A_2 + A_3)$ is the reduced mass of particle 3 with respect to the cluster (12), and $A = (A_1 + A_2 + A_3)$. Notice, $\mathbf{y}_3$ is co-linear with $\mathbf{R}_3 - \mathbf{R}_{cm}$. Alternative sets $(\mathbf{x}_1,\mathbf{y}_1)$ and $(\mathbf{x}_2,\mathbf{y}_2)$ of Jacobi coordinates are obtained by cyclic permutations of (1,2,3). We use hyperspherical coordinates $\rho, \theta, \theta_x, \phi_x, \theta_y, \phi_y$ where θ_x, ϕ_x and θ_y, ϕ_y are angles associated with unit vectors $\hat{\mathbf{x}}$ and $\hat{\mathbf{y}}$, and

$$\rho = (x^2 + y^2)^{1/2},\ \theta = \arctan(x/y). \tag{3}$$

The collective variable ρ is called the hyperradius while θ is the hyperangle. In the bound state case we seek for the three body relative motion functions in the form of the expansion

$$\Psi_{LM}(\mathbf{x},\mathbf{y}) = \rho^{-5/2} \sum_{K l_x l_y} \chi_{K l_x l_y}^{LS}(\rho) \cdot Y_{K L M}^{l_x l_y}(\Omega_5) \tag{4}$$

Here $\Omega_5 = \{\theta, \theta_x, \phi_x, \theta_y, \phi_y\}$, and $Y_{KL}^{l_x l_y}(\Omega_5)$ are hyperspherical harmonics (HH). The HH are eigenfunctions of the hypermoment operator with eigenvalues $K(K+4)$, where K=0,1,2...is referred to as the hypermoment and is the quantum number associated with the extra "angle" θ . Other quantum numbers are the Jacobi orbital momenta l_x and l_y and the total orbital moment um and its projection L, M. The HH have the following explicit form

$$Y_{KLM}^{l_x l_y}(\Omega_5) = \psi_K^{l_x l_y}(\theta) \Big[Y_{l_x}(\hat{\mathbf{x}}) \cdot Y_{l_y}(\hat{\mathbf{y}}) \Big]_{LM} \tag{5}$$

where

$$\psi_K^{l_x l_y}(\theta) = N_K^{l_x l_y} (\sin\theta)^{l_x} (\cos\theta)^{l_y} P_{\frac{K-l_x-l_y}{2}}^{l_x+1/2, l_y+1/2}(\cos 2\theta), \tag{6}$$

$P_n^{\alpha,\beta}$ are Jacobi polynomials and $N_K^{l_x l_y}$ is a normalization factor.

The corresponding Schrödinger three-body equation is

$$(T + \hat{V} - E)\Psi_{JM}^T = 0\ ,\ \hat{V} = \hat{V}_{12} + \hat{V}_{13} + \hat{V}_{23}. \tag{7}$$

After separating out the hyperangular parts of the WF we obtain a set of coupled equations similar to those for a particle moving in a deformed mean field

$$\Big(-\frac{\hbar^2}{2m}\Big[\frac{d^2}{d\rho^2} + \frac{\mathcal{L}(\mathcal{L}+1)}{\rho^2}\Big] + V_{K\gamma,K\gamma}(\rho) - E\Big)\chi_{K\gamma}(\rho) = -\sum_{K'\gamma' \neq K\gamma} V_{K'\gamma',K\gamma}(\rho)\chi_{K'\gamma'}(\rho), \tag{8}$$

$$V_{K'\gamma',K\gamma}(\rho) = < Y_{K\gamma}(\Omega_5) \mid \sum_{i<j}^{3} V_{ij}(\rho,\Omega_5) \mid Y_{K'\gamma'}(\Omega_5) >,$$
$$\gamma = \{l_x, l_y, L, S\}\ ;\ \mathcal{L} = K + 3/2. \tag{9}$$

Note that for the bound three-body states ($E \leq 0$) the hyperradial functions $\chi_{K\gamma}(\rho)$ decay exponentially at large ρ values.

It should be noticed here, that the three-body effective centrifugal barrier $\frac{\mathcal{L}(\mathcal{L}+1)}{\rho^2}$does not vanish even if the angular momenta l_x and l_y of the subsystems are equal to zero. In the case of short-range pairwise cluster interactions the three-body mean field behaves at large ρ values as $V_{K\gamma,K'\gamma'}(\rho \to \infty) \sim \rho^{-n}$ with $n \geq 3$ ($n = 3$ for the diagonal terms). This power law reflects the peculiarity of the three-body problem, namely the possibility of two particles to interact far away from the third particle.

The HHs form a complete set of functions, but to describe bound asymptotic of a binary type one may need a large series of HH . The investigations of the three-nucleon problem (see e.g. [20]) and of the ^{6}Li nucleus [1,2] have shown that for various observables involving finite distances, the convergence of the WF in hypermoment K is fast.

It should also be stressed here that in the shell model language every HH corresponds to an infinite sum of radial excitations.

3 Cluster-Cluster Interactions

α-N Interaction

Two types of α-N interactions, one of Woods-Saxon and one of Gaussian shape were tried in our previous calculations for bound and excited states of A=6 nuclei [1]. Both fit α-N scattering phase shifts satisfactorily. $V_{\alpha n}$ (WS) employs a Woods-Saxon of range 2.0 fm combined with a WS-derivative form and was used in the coordinate space Faddeev calculation for ^{6}Li [18]. The present HH calculations used the WS potential for the α-N p-wave interaction. For the s-wave component we took a purely repulsive potential with the same geometry and $V_{\alpha n} = 43$ MeV. This component of the $V_{\alpha n}$ interaction reproduces the experimental $s_{1/2}$ phase shifts well. This "Pauli core" is the way the Pauli exclusion principle is taken into account, excluding from the αN potential 0s orbits occupied by the α-core neutrons.

α-t(^{3}He) Interaction

Interaction parameters for α-t (^{3}He) were determined by analyzing the experimental data from [15],[16] on α- t (^{3}He) scattering at energies below triton break-up. The Pauli principle was simulated by repulsive cores in s- and p-waves. A number of phase equivalent potentials were tried. For final calculations we used an l-dependent potential of Gaussian shape:

$$V = V_c \exp[-(R/R_c)^2] + V_{core} \exp[-(R/R_{core})^2] - \mathbf{ls} V_{ls} \exp[-(R/R_{ls})^2]$$

The potential parameters are listed in the Tabl.1. Since all d-wave scattering phases are nearly zero up to 10 MeV , we neglected the d-wave potential in our calculations. The Coulomb interaction was taken into account.

The s- and p- phase shifts obtained with the potential from Tabl.1 are demonstrated in Tabl.2 in comparison with the erxperimental phase shifts. All phases as well as the binding energies of ^{7}Li($3/2^-$, $1/2^-$), ^{7}Be($3/2^-$, $1/2^-$), and the r.m.s. radius of ^{7}Li($3/2^-$) are reproduced well with the chosen potentials.

n- t Interaction

To determine the n+t and p+^{3}He interaction only a few experimental data on elastic scattering phases at energies below t break-up are available [14]. Therefore it is difficult to determine accurately all necessary parameters of spin-orbit and tensor interactions. We have chosen for our calculations two types of phase equivalent potentials with repulsive cores in the s-wave channel, having Gaussian and Woods-Saxon:

$$V = \frac{V_c}{1+\exp[(R-R_c)/a_c]} + \frac{V_{core}}{1+\exp[(R-R_{core})/a_{core}]} - \mathbf{ls}\frac{1}{r}\frac{V_{ls}\exp[(R-R_{ls})/a_{ls}]}{[1+\exp[(R-R_{ls})/a_{ls}]]^2}$$

shapes. The parameters of the potentials are listed in the Tabs.3,4. Tensor forces were simulated by the spin dependence of the central potentials, following e.g. paper [17]. The phase shifts are shown in the Tabs.5,6 in comparison with the experimental data. All d-wave scattering phases are small and comparable to zero at low energies, so the d-wave n-t potential was assumed to be zero in our calculations. Both choices reproduce the available n-t scattering phase shifts well within a reasonable energy range. Nevertheless, one needs more accurate experimental data to fix the potentials more precisely. This is especially important for the tensor component of the interaction, since the usual way to simulate it by a spin dependent central force does not give the correct channel coupling. Therefore, and in order to estimate the sensitivity of our calculations to the real tensor interaction, we also carried out a calculation including the nucleon-nucleon tensor forces with a free depth parameter.

4 ^{8}Li Nuclear Structure

4.1 Wave Functions

The wave functions were found using Eqs.(4), (9). Here we list the results for the WS version of the n- t potential. The binding energy for K_{max} = 2, 4 and 6 equals 0.287, 3.98 and 4.47

MeV, respectively relative to the three-particle threshold. The trend in the convergence is such that we do not expect a significant increase in the binding energy due to higher K values. Our binding energy is close to the experimental value 4.50 MeV [11]. The binding energy is, however, sensitive to uncertainties in the n-t potential: By varying that potential within experimental errors of the phase shifts we obtained a variation of the binding energy of about 200 KeV.

The predominant component of the 2^+ ground state is that with $S = L = 1$. We also see from Tabl.7 that the weights of predominant components quickly decrease as K increases. The angular momentum structure of the wave function is shown in Tabl.8 for the $n(\alpha t)$ partition. We notice that l_y=1 dominates in agreement with the p-motion adopted for the neutron in simple binary models.

In general our results confirm those of Ref. [10]. The differences in the formulations of the problem prevent us, however, from a detailed comparison.

For the first excited 1^+ level we obtained a binding energy of a 3.50 MeV relative to the three-particle threshold. Thus our calculation reproduces the experimental excitation energy of 980 keV [11] from the ground state rather well. The weights of various components of the 1^+ state are given in Tabl.9.

The second 1^+ state is lying in the two-body continuum at a calculated energy 1.58 MeV below the three-particle threshold and is slightly overbound (the experimental value relative to the three-body threshold is 1.29 MeV).

In order to investigate the sensitivity of the nuclear structure to n-t tensor forces we switched off the spin dependence of the n-t central s-wave potential and included a tensor interaction as the free nucleon-nucleon tensor interaction with a free depth parameter. This model calculation shows, that admixtures of small WF components are very sensitive to the tensor interaction. For example, by including 20% of the free nucleon-nucleon tensor force we get the same binding energy but the (l_x=1, l_y=3) WF component increases by an order of magnitude. Thus, we can conclude that it is very important to account accurately for the tensor interaction in this problem.

4.2 Matter Densities and Radii

Geometrical characteristics of the states of ^{8}Li were calculated from the wave functions. Details are described in [2]. Using r.m.s matter radii $R(^4\mathrm{He})$=1.47 fm and R(t)=1.63 fm from experiment, Tabl.10 contains various rms separations between ^{8}Li subsystems calculated for the two set of potentials described above. For the WS n-t potential good agreement with the experimental rms value $R(^8\mathrm{Li})$= 2.37±0.02 fm [19] was obtained. For the Gaussian n-t potential we obtain the same result as Ref. [10], a smaller value than in Ref. [13]. The r.m.s neutron radius, calculated for the WS n-t potential is 2.17 fm , which is less than that of Csótó [10], while the neutron skin Δr = 0.47 fm is somewhat greater than that given in Refs. [10, 13].

Our calculations indicate a 10% reduction of the ^{8}Li intercluster r.m.s. $R_{\alpha-^3H}$ separation relative to that (3.53 fm) in ^{7}Li: the valence neutron acts like "glue".

In the calculations of the matter density of ^{8}Li we correct for the sizes of the α - particle

and the triton by folding the squared wave function of their center-of-mass motion with the internal α and t densities, which we take to be Gaussians. Figs. 1-3, show the matter densities in ^{8}Li decomposed in neutron- and proton- components. The neutron density falls more rapidly than that calculated in [13], reflecting three-body dynamical features.

Additional insight is gained by plotting the correlation density (Fig. 4) (see ref. [2]) defined as the angle integrated probability $P(r_{3H-\alpha}, r_{(3H-\alpha)-n})$. The correlation plot exhibits a prominent peak at the most probable distances and qualitatively demonstrates the distortion of ^{7}Li as a function of the valence neutron distance, a characteristic feature of three-body dynamics. The calculation substantiates, however, that ^{8}Li has a structure resembling ^{7}Li + n.

5 Cross-Section of ^{7}Li(n,γ) Reaction

The cross-section of the ^{7}Li(n,γ) reaction at energies of astrophysical interest has been a subject of experimental and theoretical investigations for more than three decades. The experimental status of the reaction remains nevertheless uncertain. Three experimental values have been published at a neutron energy of about 25 keV, where only s-wave capture contributes to the cross-section. The first and largest value, obtained by Imhof et.al. at the end of the 1950s [3] is 50μb at E_n=40 keV and was reported without giving experimental errors. In this experiment the reaction was detected by observing the beta decay of ^{8}Li. Essentially the same method was used in a more recent experiment of Wiescher et.al [4], but a much lower value was obtained: $\sigma(n,\gamma)$=21.0$\pm$ 1.9 μb at E_n=25 keV. In both measurements two quantities are involved, where neither is perfectly established, namely the branching ratio to the first exited state of ^{8}Li and the probability of ^{8}Li beta decay to α + α continuum states. Another experimental method, where the reaction was detected by observing prompt γ-rays from a captured state, was used by Nagai et.al. [5]. For partial capture cross-section to the ground state of ^{8}Li they obtained: $\sigma(n,\gamma)$=35.4$\pm$ 6.0 μb at E_n=30 keV. The cross-section to the first exited state was estimated experimentally to be $\sigma(n,\gamma) \leq 9\mu$b, but was taken as 3.9$\pm$0.7 μb according to a branching ratio of 10.6$\pm$1% cited in [7] as an unpublished result. Adding these numbers, the total cross section was reported as 39.3$\pm$ 6.0 μb. The value of the branching ratio is important; the first exited state in the mirror nucleus ^{8}B lies above the two-particle threshold, hence does not contribute to the ^{7}Be(p,γ)^{8}B reaction rate. So, it is only meaningful to compare the the cross section ^{7}Li(n, γ)^{8}Li(g.s.) with that of the mirror reaction ^{7}Be(p,γ)^{8}B.

In summary the experimental situation is that the value of the ^{7}Li(n,γ) reaction cross section at low ($\approx$ 25keV) energies seems to fall within the range 20-50 μb. The previous theoretical estimates are more definite: both the simple two- body model of Barker [9] and the more refined GCM model of Descouvemont and Baye [8] support the highest value of Imhof and upper experimental limit of Nagai et.al. As we will see below, our result supports a lower value.

5.1 Two-body continuum

In the present work we use an approximate approach to the two-body continuum, which is not an exact solution of the three-body Schrödinger equation, but is simulated as a solution of a two-body equation with a ^{7}Li-n potential, fitted to reproduce observed s-wave scattering lengths and the characteristics of the ^{8}Li ground state. An attempt to account exactly for the two-body continuum in the hyperspherical harmonics method is in progress. We believe, that the essential feature of our approximate continuum solution will be retained in exact three-body calculations. The reasons for this is the following: the exact description of the two-body continuum in a three-body problem can only change this continuum in the region of the nuclear forces. The main contribution to the cross section at low energies comes however, from the near asymptotic region, where the continuum is reliably fixed by experimental values of scattering lengths. In order to compare our results with those of a two-body model we have chosen the ^{7}Li-n potentials suggested by Barker [9], which reproduce experimental s-wave scattering lengths for channel spin I=1,2. We can, however, also use other potentials, which reproduce these values since the direct radiative capture cross section at energies about 25 keV is not sensitive to details of the two-body continuum at distances inside 4.0 fm.

5.2 Results

Using (i) our three-body ^{8}Li wave function and (ii) a ^{7}Li wave function obtained as a solution of a two-body Schrödinger equation with the same α $-^3$ H potential, and (iii) the wave function for ^{7}Li-n relative motion in Barker's potential, we calculated the s-wave direct neutron capture cross section. All necessary formulas are given in the Appendix. The final result : at E_n=25 keV partial capture cross-section to the $\sigma(n,\gamma)^8Lig.s.$ =27.5 μb, total $\sigma(n,\gamma)$=28.2 μb (with a branching of 0.7μb to the first excited state). Thus our three-body approach, leads to the partial cross section to the ^{8}Li ground state which is slightly below the lower experimental limit of Nagai et.al. $\sigma(n,\gamma)$=35.4$\pm$ 6.0 μb[5], while the total cross-section is more smaller than that derived in [5] due to the small branching to the first excited state. This value is essentially smaller than the two body cross section of Barker ($\sigma(n,\gamma) \approx 50\mu$b) [9] and the GCM results [12] (54.9-44.5 μb) . The reason for such difference is the different asymptotic behaviour of the ^{8}Li wave functions in three-body and two-body approaches. For both cases the region below 3 fm does not contribute to the cross section because of nature of the dipole operator, suppresing small distances, and the lack of resonant states in the vicinity of this energy region. For the three-body case the cross section grows rapidly between 4-8 fm and saturates at $\approx$ 11 fm in hyperradius . It should be mentioned here that we solve the three body Schrödinger equation exactly up to 15 fm and match this solution with the three body asymptotics from 15 fm. Since the saturation of the three-body cross section occurs at 11 fm and the convergence of the ^{8}Li WF in hypermoment K is quite good (see Tabl.7), we don't expect a significant contribution from explicitly accounting for the two-body channel in the three-body problem.

6 Conclusion

We have performed a detailed study of ^{8}Li which, aside for its own role in nucleosynthesis also is a mirror nucleus to the more complicated ^{8}B, and may thus provide a key to nuclear aspects of the Solar neutrino problem. A three-body model with realistic interactions between the clusters, which reproduce all observables in binary subsystems was developed. Without fitting parameters we could for the first time reproduce the binding energy in a satisfactory way and also the splitting between the 2^+ ground state and 1^+ first excited state, as well as the matter radius of the ^{8}Li ground state.

Analysis of pair interactions showed that the main ingredients of calculations, i.e. ^{4}He+t and ^{4}He+n two-body potentials, are well-established. But to reproduce fine details of ^{8}Li spectra and some components in the ground state wave function , that could give a few-percent correction to the cross-section we are strongly in need of experimental information on n-t phase shifts to reconstruct non-central components of n-t interaction (ls- and tensor forces).

Using three-body wave functions for the ground state and 1^+ state of ^{8}Li we have investigated the ^{7}Li (n,γ) reaction at 25 keV with a variety of continuum wave functions, fixed by experimental phase analysis in binary models. Due to the three-body characteristics of the ^{8}Li nucleus our result is a ^{7}Li (n,γ) partial cross section to the ^{8}Li ground state of 27.5 μb at neutron energy 25 keV, supporting the lower limit of the experimental value 35.4$\pm$ 6 μb [5] and the ^{7}Li (n,γ)^{8}Li(1^+) of 0.7 μb.

The ^{7}Li (n,γ) cross-section depends only weakly on the way we construct the continuum wave function, as long as it satisfies asymptotic experimental phase shifts. In contrast it is very sensitive to the behaviour of the ^{8}Li wave function in the nuclear exterior.

For the mirror reaction ^{7}Be (p,γ), where the asymptotic behaviour of $^8B_{g.s.}$ wave function may be even more important, we also expect a reduction of the cross-section at the energies of astrophysical significance. Work on this reaction is in progress. The extended HH theory with inclusion of the binary channels, or Faddeev equations are the most promising tools for answering this nuclear physics question.

7 Acknowledgments

This work was done under the financial support from NORDITA, NBI, the Danish National Scientific Research Council and the International Science Foundation (grant N M7C000). One of the authors (V.E.) is thankful to The Niels Bohr Institute for hospitality. N.S. and B.D. are grateful to Yu.Gaponov for useful discussions.

8 Appendix

The ^{7}Li (n,γ) cross-section is calculated using the well known formula (we assume $\hbar$=c=1):

$$\sigma = \frac{16\pi e^2 E_\gamma^3}{9v(2j_x^i+1)(2s_y^i+1)} \sum_{M,M_f,I,M_I} |\langle f|T^\epsilon_{1M}|i\rangle|^2 \tag{10}$$

In N-cluster representation the standard dipole operator (referred to the CM) is

$$T^\epsilon_{1M} = \sum_{i=1}^N z_i r_i Y_{1M}(\hat{r}_i)$$

In case of three charged clusters it takes the form (the Jacobi coordinates are defined in sect. II)

$$\begin{aligned} T^\epsilon_{1M} &= z'_y y Y_{1M}(\hat{y}) + z'_x x Y_{1M}(\hat{x}) \\ &= z'_y \rho\cos\theta\, Y_{1M}(\hat{y}) + z'_x \rho \sin\theta\, Y_{1M}(\hat{x}) \end{aligned}$$

with effective charges

$$z'_x = \sqrt{\frac{A_1A_2}{A_1+A_2}}\left(\frac{z_2}{A_2}-\frac{z_1}{A_1}\right) \tag{11}$$

$$z'_y = \sqrt{\frac{(A_1+A_2)A_3}{A_1+A_2+A_3}}\left(\frac{z_1+z_2}{A_1+A_2}-\frac{z_3}{A_3}\right) \tag{12}$$

(A_i is the mass number of a cluster).

For electromagnetic capture we use a WF for the initial state of n+^{7}Li in the channel spin (I) representation (the relative motion momentum **k** is along the z-axis), which in corresponding Jacobi coordinates takes the form

$$\Psi_i(x,y) = \sum_{l^i_y} (i)^{l^i_y}\sqrt{4\pi(2l^i_y+1)} \sum_{J_i,M_i} |(l^i_x s^i_x)j_x(j_x s^i_y)I(l^i_y I)J_iM_i\rangle \frac{\phi^i_{l^i_y}(k'y)}{k'y}\frac{\phi^i_{l^i_x}(x)}{x} e^{i\delta}\langle IM_I l^i_y 0|J_iM_i\rangle$$

In the above a natural normalization of the scattering wave function and the bound state wave function was assumed. Namely, at $y\to\infty$

$$\phi^i_{l^i_y}(k'y) \to \sin(k'y+\delta),$$

and

$$\int_0^\infty dx(\phi^i_{l^i_x}(x))^2 = 1.$$

Transforming this WF to L-S coupling gives for the spin-angular part ($\hat{J}=\sqrt{2J+1}$)

$$\begin{aligned} |(l^i_x s^i_x)j_x(j_x s^i_y)I(l^i_y I)J_iM_i\rangle = \sum_{L_iS_i} (-1)^{L_i+l^i_x+l^i_y}\hat{j}^i_x\hat{L}_i\hat{I}\hat{S}_i\, W(l^i_x s^i_x I s^i_y; j^i_x S_i) \\ W(S_i l^i_x J_i l^i_y; I L_i)\,|(l^i_x l^i_y)L_i(s^i_x s^i_y)S_i(L_iS_i)J_iM_i\rangle \end{aligned}$$

After integration over angles $\hat{x}$ and $\hat{y}$ the transition matrix element between the two-body L-S coupled continuum wave function and the ground state WF of ^{8}Li can be written as

$$\langle J_f M_f \pi_f | T^e_{1M} | J_i M_i \pi_i \rangle = \langle 1 M J_i M_i | J_f M_f \rangle \sum_{\gamma_i \gamma_f K_i K_f} \sqrt{\tfrac{3}{4\pi}} (-1)^{J_f + S_f + l^f_x + \vec{l}^i_y} \hat{l}^i_y \hat{L}_i \hat{\vec{L}}_i \hat{J}_i \langle 10 l^i_y 0 | \vec{l}^i_y 0 \rangle \begin{Bmatrix} 1 & l^i_x & \vec{l}^i_y \\ l^i_y & \vec{L}_i & L_i \end{Bmatrix} \begin{Bmatrix} 1 & L_i & \vec{L}_i \\ S_i & J_f & J_i \end{Bmatrix}$$

$$\langle \phi_{K_f \gamma_f}(\rho, \theta) | z'_y \rho \cos\theta | \frac{\phi^{l^i_y}_{l^i_y}(k'y)}{k'y} \frac{\phi^{l^i_x}_{l^i_x}(x)}{x} \rangle$$

with selection rules $l^i_x = l^f_x$, $\vec{l}^i_y = l^f_y$, $\vec{l}^i_y = l^i_y \pm 1$, $\vec{L}_i = L_i, L_i \pm 1$, $\vec{L}_i = L_f$

The spin-angular integration over $\hat{x}$ is performed by interchanging the x and y indices taking into account additional phase multipliers $(-1)^{-L_i + l^i_x + l^i_y}$ and $(-1)^{-L_f + l^f_x + l^f_y}$ after this permutation.

Radial matrix elements

$$\langle \phi_{K_f \gamma_f}(\rho, \theta) | z'_y \rho \cos\theta | \frac{\phi^{l^i_y}_{l^i_y}(k'y)}{k'y} \frac{\phi^{l^i_x}_{l^i_x}(x)}{x} \rangle$$

are calculated numerically with a quasi-gaussian 200 points formula for the hyperangular part that we used in the matrix element calculations. A hyperradial grid with step 0.2 fm was chosen for the solution of coupled hyperradial equations for $K_{max} \leq 4$. For K_{max} up to 6 these equations were solved by expansion in a convenient set of hyperradial functions (see e.g. [20]). The two methods lead to the same results for $K_{max} \leq 4$.

References

[1] M.V.Zhukov, B.V.Danilin, D.V.Fedorov, J.M.Bang, I.J.Thompson, J.S.Vaagen, Phys.Rep. v.**231** (1993) 151

[2] B.V.Danilin, M.V.Zhukov, A.A.Korsheninnikov, L.V.Chulkov, V.D.Efros, Sov. Jour. Nucl. Phys. **49** (1989) 351,359; ibid **53** (1991) 71; B.V. Danilin, M.V. Zhukov, S.N. Ershov, F.A. Gareev, R.S. Kurmanov, J.S. Vaagen and J.M. Bang, Phys. Rev. **C43** (1991) 2835

[3] W.L.Imhof et.al., Phys.Rev. **114** (1959) 1037

[4] M.Wiescher et.al., Astroph.J. **A344** (1989) 464

[5] Y.Nagai et.al., Astroph.J. **A381** (1991) 444

[6] R.A. Malaney and W.A.Fowler, Astroph.J. **A333** (1988) 14

[7] F. Ajzenberg-Selove and T.Lauritsen, Nucl. Phys. **A227** (1974) 1

[8] P.Descouvemont, D.Baye, Nucl.Phys. **A567** (1994) 341

[9] F.C.Barker, Aust.J.Phys. **33** (1980) 177

[10] A.Csótó, Phys.Lett. **B315** (1993) 24

[11] F.Ajzenberg-Selove, Nucl. Phys **A490** (1988)1

[12] P.Descouvemont, J.Phys. **G19** (1993) S141

[13] D.Baye, P.Descouvemont and N.K.Timofeyuk, Nucl. Phys. **A577** (1994) 624

[14] T.A.Tombrello, Phys. Rev. **143** (1966) 772

[15] W.R.Boykin, S.D.Baker and D.M.Hardy, Nucl. Phys.**A195** (1972) 241

[16] D.M.Hardy et.al., Nucl. Phys.**A195** (1972) 250

[17] S.V.Dubovichenko and A.V.Dzhazairov-Kakhramanov, Yad. Phys. (Soviet) **56** (1993) 45

[18] J.Bang et.al., Nucl. Phys. **A405** (1983) 126

[19] I.Tanihata et.al., Phys. Lett. **B206** (1988) 592

[20] M.I.Mukhtarova, Yad. Phys. (Soviet) **49** (1989) 338

	V_c MeV	R_c fm	V_{core} MeV	R_{core} fm	V_{ls} MeV	R_{ls} fm
s-wave	-	-	80	2.1	-	-
p-wave	-141.6	2.1	300	1.43	2.3	2.1
f-wave	-48.5	3.1	-	-	13.2	1.91

Table 1: Parameters of α-t Gaussian potentials.

E(MeV)	$\delta^+_{1/2}$ ex.	$\delta^+_{1/2}$th.	$\delta^-_{1/2}$ ex.	$\delta^-_{1/2}$th.	$\delta^-_{3/2}$ ex.	$\delta^-_{3/2}$ th.
3.30	-23± 2	-21.6	162± 3	162.1	165± 1	163.7
3.51	-24± 1	-23.6	161± 1	160.3	164± 1	162.1
3.88	-27± 1	-27.0	159± 2	157.3	162± 1	159.3
4.37	-30± 1	-31.4	156± 2	153.5	158± 1	155.6
4.46	-31± 1	-32.2	156± 2	152.8	158± 1	154.9
4.64	-33± 2	-33.8	153± 2	151.4	158± 1	153.6
4.79	-34± 1	-35.1	151± 2	150.3	157± 2	152.5
4.95	-40± 6	-36.4	150± 3	149.1	154± 2	151.4
5.09	-49± 7	-37.6	146± 5	148.1	153± 3	150.4
5.21	-38± 5	-38.6	149± 3	147.2	153± 2	149.5
6.04	-50± 7	-45.3	137± 5	141.5	142± 2	143.9
6.46	-49± 5	-48.4	139± 3	138.7	140± 2	141.2
6.86	-48± 9	-51.4	139± 4	136.1	140± 4	138.7

Table 2: Phase shifts (degrees) for p-wave α - t scattering. Experimental data are taken from Ref.[16].

	V_c MeV	R_c fm	a_c fm	V_{core} MeV	R_{core} fm	a_{core} fm	V_{ls} MeV· fm	R_{ls} fm	a_{ls} fm
s-wave,S=0	-33	2	0.7	200	1.43	0.7	-	-	-
s-wave,S=1	-33	2	0.7	400	1.43	0.7	-	-	-
p-wave,S=0	-43	2	0.7	-	-	-	-	-	-
p-wave,S=1	-33	2	0.7	-	-	-	66	1.5	0.35

Table 3: Parameters of N-t (^{3}He) WS potentials.

	V_c MeV	R_c fm	V_{ls} MeV	R_{ls} fm
s-wave,S=0	160	2.1	-	-
s-wave,S=1	220	2.1	-	-
p-wave,S=0	-8.8	3.725	-	-
p-wave,S=1	-18.6	3.015	4.67	3.015

Table 4: Parameters of N-t (^{3}He) Gaussian-potentials.

E(MeV)	δ_{110} ex.	δ_{110}th.	δ_{011} ex.	δ_{011}th.	δ_{111} ex.	δ_{111} th.	δ_{211}ex.	δ_{211}th.
1	5.7	3.4	3.0	2.5	11.1	3.1	8.1	6.1
2	17.6	9.7	4.8	7.1	16.2	8.8	30.6	19.3
3.5	25.0	21.7	7.0	14.9	29.0	19.2	53.2	45.2
6	24.9	39.3	14.3	26.1	48.9	34.0	65.1	71.4

Table 5: Phase shifts (degrees) for p-wave n-t scattering (WS-potential).

E(MeV)	δ_{000} ex.	δ_{000}th.	δ_{101} ex.	δ_{101}th.
1	-26.6	-26.0	-36.2	-32.4
2	-36.1	-36.3	-45.5	-45.4
3.5	-47.0	-47.5	-59.2	-59.3
6	-60.7	-60.6	-76.2	-76.3

Table 6: Phase shifts (degrees) for s-wave n-t scattering (WS-potential).

K	$S=1, L=1$	$S=1, L=2$	$S=1, L=3$	$S=0, L=2$
2	85.5	0.8	-	0.3
4	10.7	1.1	0.05	0.37
6	1.0	0.1	0.05	0.1
Σ	97.2	2.0	0.1	0.7

Table 7: Percentage of various L, S components of the ground-state wave function of ^{8}Li.

L	S	l_x	l_y	WF percentage (HH)	WF percentage [10]
1	1	1	1	96.1	95.0
2	1	1	1	1.1	1.9
2	0	1	1	0.4	1.6
2	1	3	1	0.8	2.0
2	1	1	3	0.2	0.09
2	0	3	1	0.18	1.6
2	0	1	3	0.02	0.03

Table 8: Weights of the main components of the ground-state wave function of ^{8}Li. l_x is the relative $\alpha - t$ orbital momentum and l_y - the neutron orbital momentum relative to (αt).

K	$S=1, L=1$	$S=0, L=1$	$S=1, L=0$	$S=1, L=2$
2	15.1	72.4	0.03	0.9
4	1.7	7.3	0.13	1.10
6	0.17	0.8	0.03	0.11
Σ	17.0	80.5	0.2	2.2

Table 9: Percentage of various L, S components of the first exited state of ^{8}Li.

J:	2^+	2^+	1^+	1^+
t-n pot. :	Gauss	WS	Gauss	WS
$\overline{r_{n-7Li}}$	4.00	3.63	4.14	3.88
$\overline{r_{3H-\alpha}}$	3.26	3.13	3.27	3.23
$\overline{r_n^{CM}}$	3.50	3.17	3.63	3.40
$\overline{\rho}$	5.67	5.32	5.78	5.58
$\overline{R_{matter}}$	2.45	2.35	2.48	2.42

Table 10: Calculated r.m.s. separations between various parts of the ^{8}Li system. The experimental value is R^{exp}_{matter}=2.37± 0.02 fm [19].

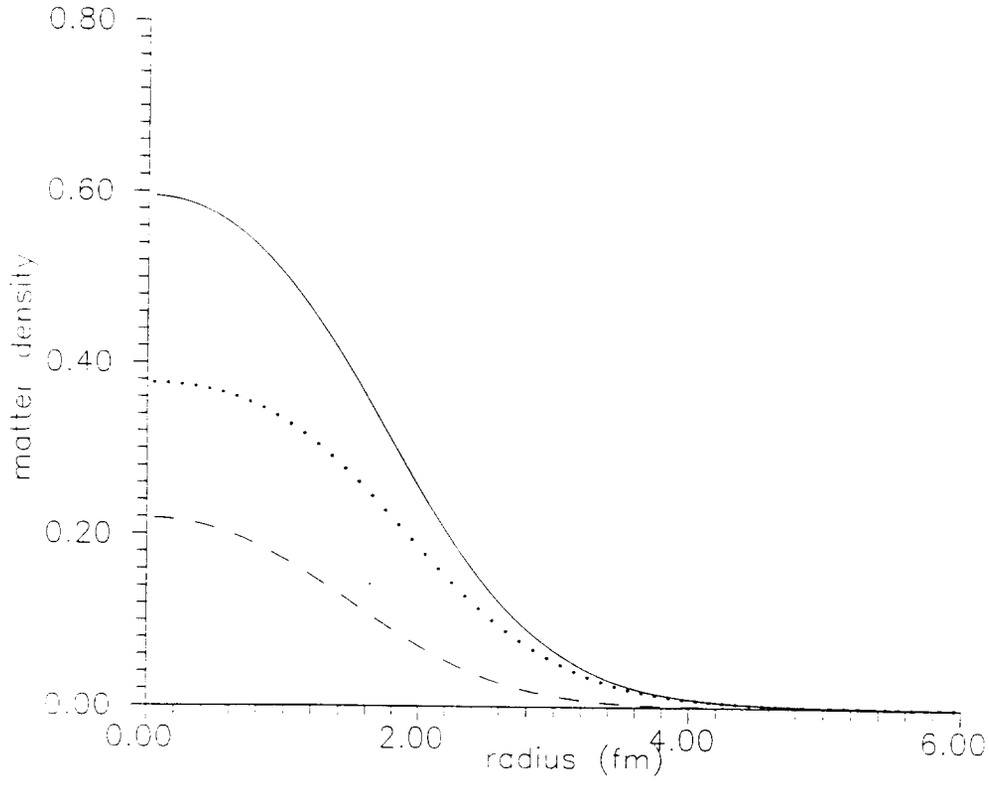

Fig.1 Matter density of 8Li ground state
dashed line – protons, dotted line – neutrons,
solid line – total

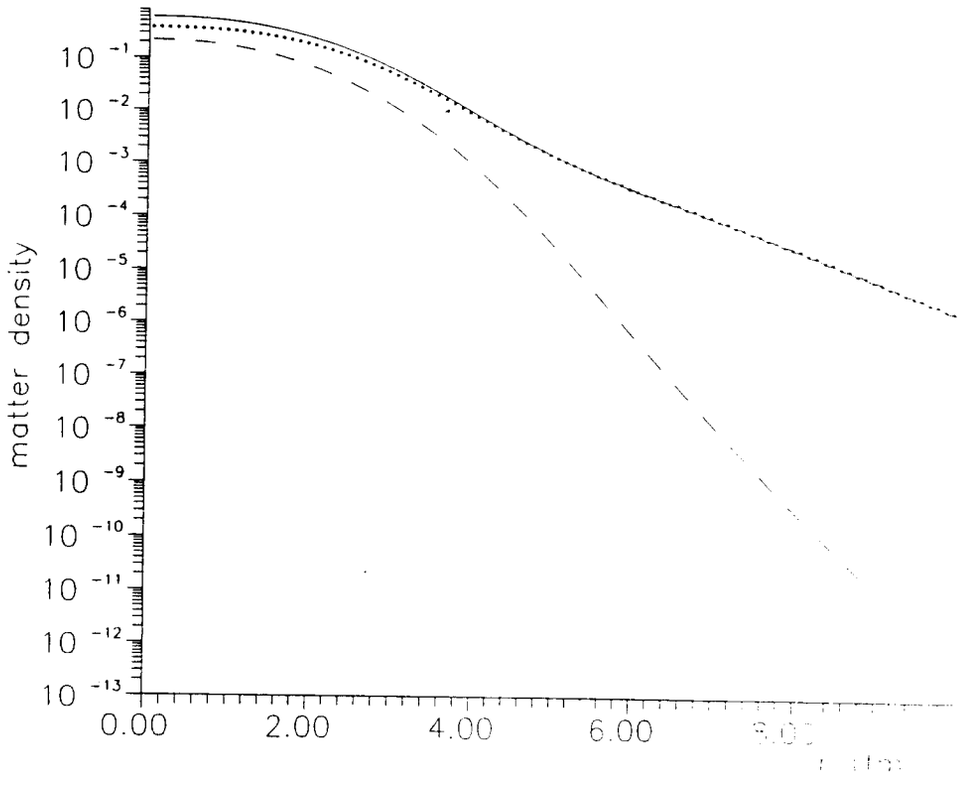

Fig.2 Matter density of 8Li ground state
dashed line – protons, dotted line – neutrons,
solid line – total

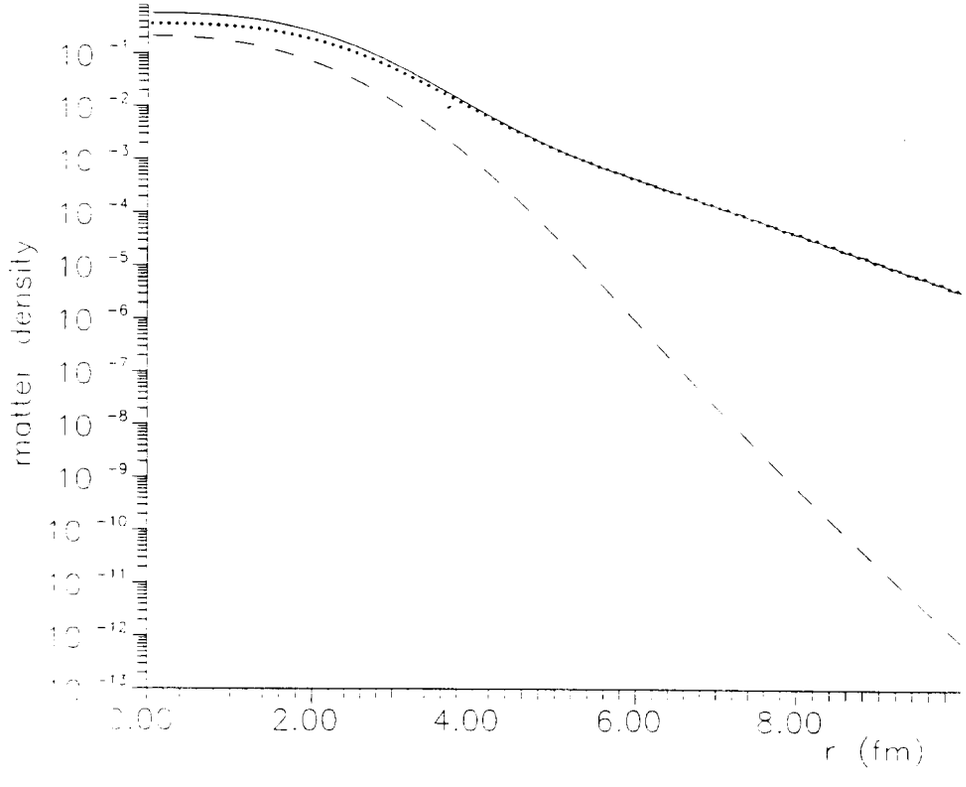

Fig.3 Matter density of 8Li first excited state
dashed line – protons, dotted line – neutrons,
solid line – total

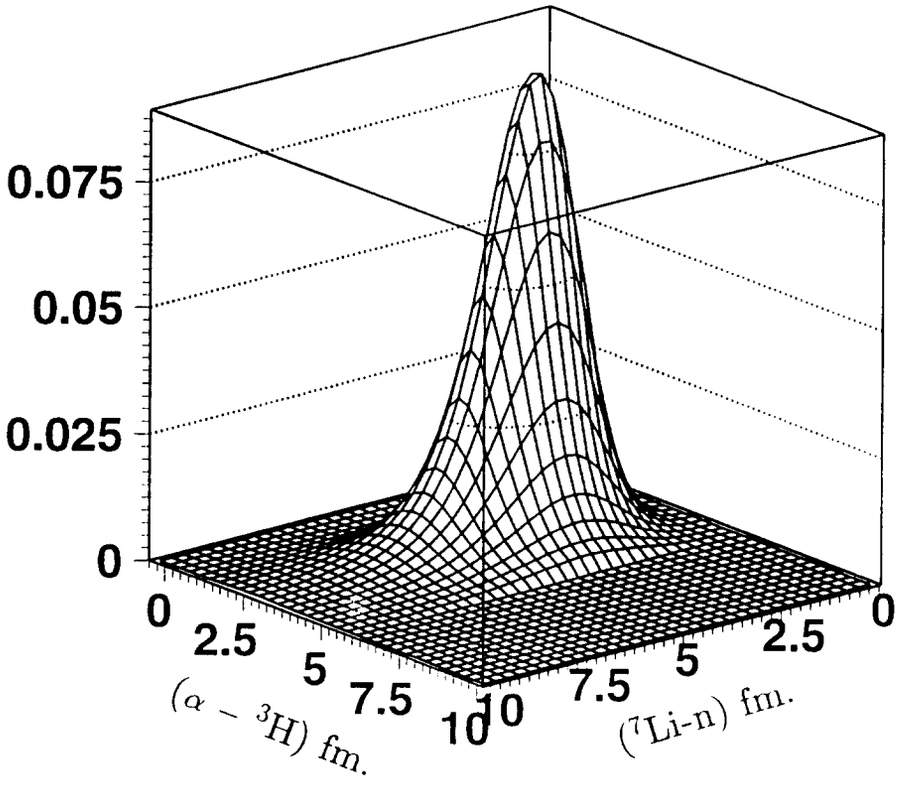

Fig.4 ^{8}Li spatial density.